ARTICLE

DOI: 10.1590/2317-4889202020190087

BJGEO
Brazilian Journal of Geology

Oxygen fugacity of Alto Paranaíba kimberlites and diamond instability: Três Ranchos IV and Limeira I intrusions

Bruna Coldebella[1], Rogério Guitarrari Azzone[1]*, Luanna Chmyz[1], Excelso Ruberti[1], Darcy P. Svisero[1]

Abstract

Oxygen fugacity (fO_2) conditions were established for Três Ranchos IV (TR-IV, diamond-bearing) and Limeira I (LM-I, barren) kimberlite intrusions, in Alto Paranaíba Alkaline Province, to constrain a possible correlation between fO_2 and diamond instability. Temperature and pressure estimates obtained from the xenocryst assemblage composition are compatible up to garnet lherzolite levels. It suggests that both intrusions could cross the diamond-stability field. The fO_2 of the TR-IV constrained by perovskite oxygen barometry presents an average value of -2.4 for ΔNNO, with standard deviation of 1.30 (n = 120), whereas those calculations for LM-I have an average value of -1.31 for ΔNNO, with standard deviation of 1.38 (n = 81). Considering these uncertainties, there is an important superposition of fO_2 values for both intrusions, in which there is higher tendency of more reduced conditions for TR-IV. For the LM-I, an oxybarometer based on the composition of monticellite yielded a similar ΔNNO range: -4.2 and +2.5. Some crystals and samples present trends towards more reduced conditions, while others display more oxidized conditions for each intrusion. Due to the superposition of ranges and absence of a preferential trend, the influence of fO_2 for the possible instability of diamonds in the study area remains uncertain.

KEYWORDS: kimberlites; Alto Paranaíba Province; intensive parameters of crystallization; oxygen fugacity.

INTRODUCTION

Kimberlites are of remarkable scientific and economic relevance for providing a better understanding about the genesis and evolution of primitive magmas and for carrying diamonds, as they are emplaced into the upper crust (Mitchell 1995). Those rocks record the highest known oxygen fugacity values of terrestrial magmas, which is a phenomenon related to the presence of deep oxidized sources and to the interaction of ferrous iron and carbon-fluid equilibrium during ascent (Canil and Bellis 2007). The fO_2 of kimberlites mainly reflects the conditions of their source regions (Carmichael 1991). Thus, this type of magma provides environmental information from depths greater than 200 km, as evidenced by the xenocrysts they bear. Moreover, in some cases, the oxygen fugacity of kimberlite magmas can partially control the quality and presence of diamonds in these rocks (Canil and Fedortchouk 2001, Fedortchouk *et al.* 2005). Detailed petrographic studies revealed that perovskite may be crystallized during a long-time span in the evolution of kimberlite magmas (*i.e.* soon after the macrocrystal phases to late-stage magmatic degassing), over a large range of P-T conditions (Sarkar *et al.* 2013). Due to such protracted crystallization history of perovskite, this oxybarometer can potentially indicate, in great details, the fO_2 recorded during the formation and emplacement of the kimberlite in different magma batches and/or eruption phases (Chakhmouradian and Mitchell 2000).

It is also known that other intensive variables (*e.g.* P-T) may have an important role in the presence of diamonds in kimberlites. As highlighted by Ogilvie-Harris *et al.* (2009), during the ascent of kimberlite magmas, processes such as decompression (Carmichael and Ghiorso 1986), cooling, degassing, assimilation of crustal and mantle minerals (Sparks 2013), crystallization (Carmichael and Nicholls 1967), and interaction with crustal fluids (Ogilvie-Harris *et al.* 2009) may cause significant variations in pressure, temperature, volatile content, and oxygen fugacity (Ballhaus and Frost 1994). Such variations in the intensive parameters may cause, in turn, changes in mineral assemblages, mineral and melt compositions and physical properties of magmas (Ogilvie-Harris *et al.* 2009).

The ultrabasic and mainly potassic rocks generated by the Cretaceous alkaline magmatism, which took place in the central and southeastern portions of the Brazilian platform, are important for understanding the composition and evolution of the lithospheric and sub-lithospheric mantle in the region, based on the study of xenoliths and xenocrysts samples from

Supplementary data

Supplementary data associated with this article can be found in the online version: Supplementary Material A, Supplementary Material B, Supplementary Material C, and Supplementary Material D.

[1]Programa de Pós-Graduação Geociências (Mineralogia e Petrologia), Instituto de Geociências, Universidade de São Paulo – São Paulo (SP), Brazil. E-mails: brunacoldebella@usp.br, rgazzone@usp.br, chmyz@usp.br, exrubert@usp.br, svizzero@usp.br

*Corresponding author.

these magmas (*e.g.*, Meyer and Svisero 1980, Gonzaga and Tompkins 1991, Leonardos and Meyer 1991, Bizzi *et al.* 1994, Meyer *et al.* 1994, Carlson *et al.* 1996, Brod *et al.* 2000, Araújo *et al.* 2001, Junqueira-Brod *et al.* 2002, 2004). Despite numerous studies, the petrological constraints from some classical occurrences remain poorly understood, especially in Alto Paranaíba Alkaline Province (APAP), where mantle xenoliths and xenocrysts are abundant.

Among the hundreds of known kimberlite intrusions in Alto Paranaíba region, only 18 have been estimated to be diamond-bearing occurrences (Cabral Neto *et al.* 2017). Some of the reasons that could explain the presence of diamonds only in a few bodies are: depths at which magmas are formed; variations in oxygen fugacity conditions that would lead to greater unstabilization of the diamonds carried by these magmas; and local mantle heterogeneities, which would allow sampling of certain minerals (such as diamond) possibly absent in other portions.

The main question of this study regards the influence that oxygen fugacity might have had on the instability of carried (or possibly carried) diamond xenocrysts when barren- and diamond-bearing kimberlite intrusions from APAP were compared with each other. As detailed study targets, we selected the Três Ranchos IV (TR-IV) intrusion, which is known to be a microdiamond-bearing intrusion, and the barren Limeira I (LM-I) intrusion. In addition, we discuss some possible implications associated with the diamond potential of these intrusions. This is a pioneering study of APAP rocks and the first approach to quantify the oxygen fugacity from cognate phases and to discuss the implications of the variation of this intensive parameter.

GEOLOGICAL SETTING

More than 100 alkaline bodies of Permian-Triassic to Paleogene age are known in the central and southeastern Brazilian Platform, especially those close to the limits of Paraná Basin (Riccomini *et al.* 2005). Almeida (1983) introduced the concept of alkaline province for alkaline bodies clusters of similar petrographic, age and tectonics and, later, 15 provinces were defined in the central-southeastern Brazilian Platform (Riccomini *et al.* 2005). Among them, the APAP (Fig. 1) is one of the largest

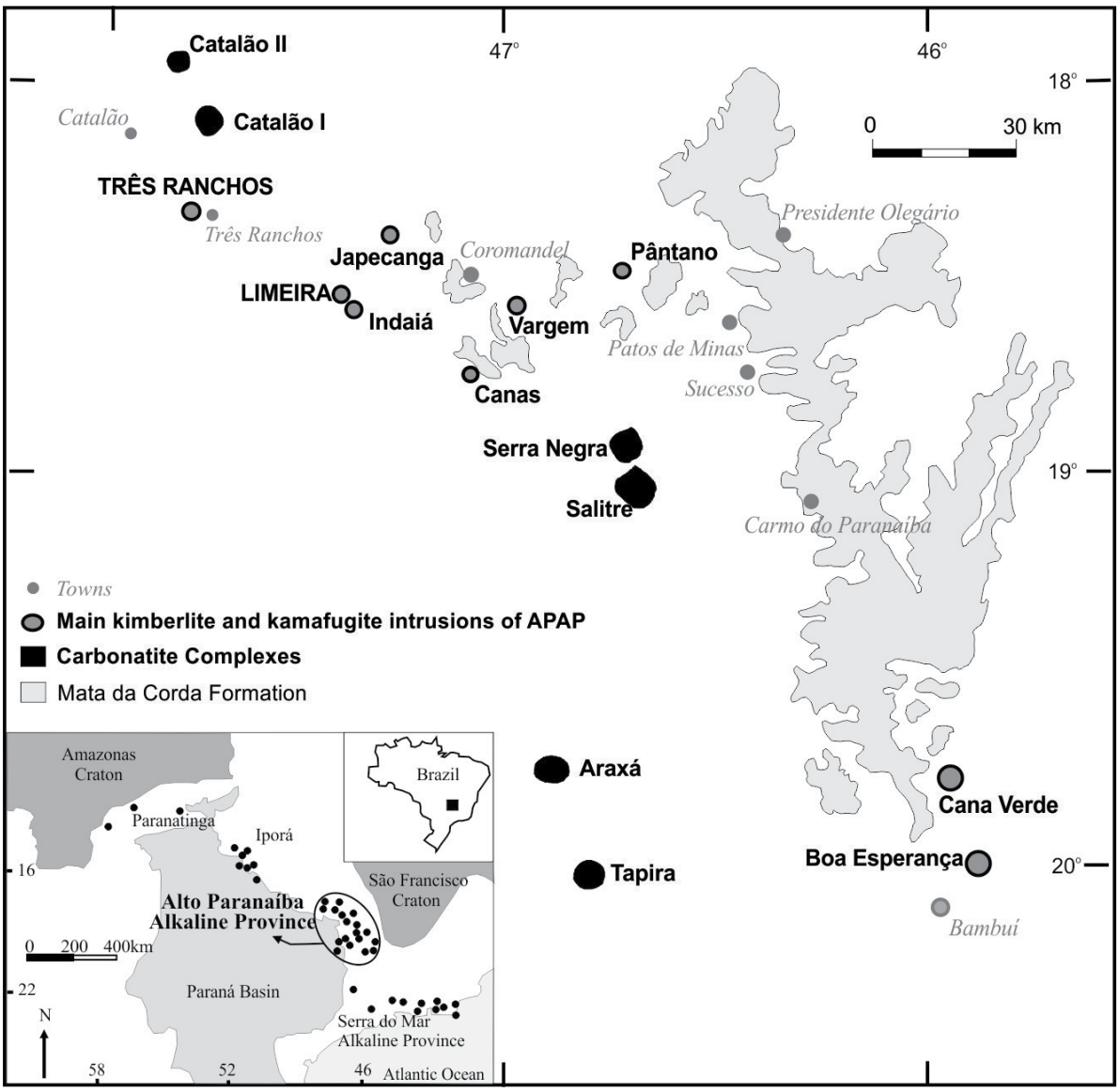

Figure 1. Sketch map of Alto Paranaíba Alkaline Province (APAP) and Mata da Corda Formation, following Meyer *et al.* (1994). The inset presents the APAP relationships with the main Brazilian structural domains (Gibson *et al.* 1995b).

potassic-ultrapotassic provinces in the world (> 15,000 km^3; Gibson *et al.* 1995a, 1995b, Brod *et al.* 2000, Araújo *et al.* 2001, Comin-Chiaramonti and Gomes 2005), consisting of a diversity of ultrabasic and ultrapotassic rock types (*i.e.*, kimberlites, lamproites and large volumes of kamafugite lava flows) and several plutonic alkaline complexes with associated carbonatites (Brod *et al.* 2000). Most of the rocks show an economic potential for precious minerals and industrial applications, such as diamonds in kimberlite occurrences or P, Nb, Ti, REE (rare earth elements) that occur as residual and supergene enrichments over carbonatite complexes (Biondi 2005).

In the APAP, Coromandel-Três Ranchos kimberlitic field (Cabral Neto *et al.* 2017) covers an area of approximately 11,600 km^2 within APAP and includes more than 500 kimberlitic intrusions. They usually show structures of pipes up to 300 ha large (*e.g.*, Japecanga-6 kimberlite), as well as hypabyssal, diatreme and craters facies in several occurrences. Bodies showing hypabyssal facies features include TR-IV and LM-I kimberlites (Svisero *et al.* 1980, Svisero *et al.* 1984, Meyer *et al.* 1994, Costa *et al.* 1997) that are described as: TR-IV occurs as blocks in an area of approximately 0.5 ha and, according to Costa *et al.* (1997), this kimberlite intrudes granitic rocks, quartzites, schists, and amphibolites of Araxá Group, which occur as xenoliths; LM-I, also named Perdizes 04a (Cabral Neto *et al.* 2017), occurs as blocks and boulders in an area of ~3.5 ha, intruding the basement and has not been reported to bear diamonds.

INTENSIVE PARAMETERS ON ALTO PARANAÍBA KIMBERLITES: PREVIOUS WORKS

Several works have reported pressure and temperature estimations obtained from xenoliths of APAP. Leonardos *et al.* (1993) calculated intervals of 977 to 1,273°C for TR-IV kimberlite temperature, a pressure ranging from 55.5 to 78 Kbar, and a geotherm that approaches a 40 W/m^2 heat flow model (for a steady-state conductive lithosphere), using diopside and Cr-diopside from a garnet lherzolite xenolith. By applying several geothermobarometers from TR-IV xenoliths, Costa (2008) presented a temperature range of 974 to 1,139°C, a pressure range of 36 to 51 Kbar, and geotherms of about 38 and 63 mW/m^2. For LM-I kimberlite xenoliths, Almeida (2009) introduced temperatures ranging from 622 to 921°C that were obtained from orthopyroxene, clinopyroxene, olivine, and spinel geothermometers. A compilation of geochemical data from several publications on the APAP allowed Cabral Neto *et al.* (2017) to determine, from the clinopyroxene geothermobarometer of Nimis and Taylor (2000), a geotherm ranging from 40 to 50 mW/m^2 for the lithosphere related to the LM-I kimberlite and 35 to 40 mW/m^2 for TR-IV. Read *et al.* (2004) introduced an important approach to single grain thermobarometric methods for mantle-derived xenocrystic clinopyroxene derived from kimberlite samples of APAP. Spinel-facies clinopyroxenes occur predominantly in the temperature interval between 625 and 875°C, overlapping the lower end of the 700–1,000°C temperature range, in which garnet-facies clinopyroxenes predominate (Read *et al.* 2004). A geotherm close to 37 mW/m^2 is proposed, which is close to the heat flow model for steady-state conductive lithosphere (Pollack and Chapman 1977).

SAMPLES AND ANALYTICAL TECHNIQUES

Thirty-four thin sections from LM-I and TR-IV kimberlites were analyzed in order to identify the mineral assemblages and xenocrysts present and to estimate their modal volumes (Mitchell 1986, 1995, Le Maitre 2002). Photomicrographs were taken in the Petrographic Microscopy Laboratory (GeoAnalítica-USP), using a Zeiss Axio Imager A2m microscope coupled to an AxioCam MRc digital camera. Five polished thin sections (80 μm-thick) from TR-IV and seven from LM-I were analyzed in a FEI Quanta 600F scanning electron microscope under a 20kV accelerating voltage in the Technological Characterization Laboratory of the Department of Mining and Petroleum Engineering, Polytechnic School, at Universidade de São Paulo (USP). A 20-25 ηm carbon coat was applied to every sample before analysis. High-resolution backscattered electron (BSE) images were taken to identify any zoning or fracturing present and to establish the textural relationships in mineral phases as ilmenite, spinel, olivine, perovskite, magnetite, and monticellite.

Mineral chemistry data were acquired in the Electron Microprobe Laboratory of Geo-analytics from USP, with a JEOL JXA-8530 Electron Probe Microanalyzer (EPMA). Natural and synthetic standards were applied. Ten samples were covered with a 20–25 ηm carbon coat in an EDWARDS AUTO 306 evaporator prior to EPMA analyses. Five spectrometers were used to assess these elements. Perovskite grains were analyzed under an accelerating voltage of 25 kV and an emission current of 100 ηA for better quantification of REEs, minor and trace element analysis. Major elements of monticellite, olivine, pyroxene, spinel, garnet, and ilmenite were measured under an accelerating voltage of 15 kV and an emission current of 20 ηA. Matrix corrections were performed with CITZAF (Armstrong 1995) and ZAF algorithms. The EPMA data for the analyzed minerals are listed in Supplementary Material A.

The concentrations of trace elements and REE were analyzed at Geoanalítica-USP Chemistry Laboratory by laser ablation inductively coupled plasma mass spectrometer (LA-ICP-MS) in olivine, garnet, perovskite, and pyroxene. A Thermo Scientific™ iCAP™ RQ ICP-MS coupled with a New Wave UP213nm laser was used. Helium was applied as a carrier gas of the ablated sample into the Ar plasma. NIST-612 (glass), BHVO (basalt), and BIR (glass) calibration standards were applied to all samples. Analytical procedures were performed according to Andrade *et al.* (2014). A total of eight polished thin sections were selected, four from each kimberlite intrusion. Primary data reduction and normalization were performed with Glitter v.4.0 (Macquarie University), using reference values from GEOREM website for calibration standards. Ca was used as internal standard for perovskite, and Si for olivine. The concentrations of the selected elements were analyzed previously by EPMA. The LA-ICP-MS results for the analyzed phases, as well as the standard mass spectrometer

and laser setup of a typical session, are given in Supplementary Material B.

Studies on Brazilian kimberlites are hampered by the scarcity of fresh outcrops due to intense tropical weathering. In the investigated bodies, un-weathered rocks are only found as rare boulders and blocks close to the drainage network. We have collected fresh samples from each kimberlite intrusion (TR-IV and LM-I — see detailed petrographic description below), and these materials were carefully hand-picked in order to avoid any weathered portions. The samples were then crushed for whole rock geochemical analyses, firstly in a steel jaw crusher, then in a disk mill of agate. Subsequently, each powdered sample was used to prepare pressed pellets and fused beads for X-ray fluorescence analysis, and chemically dissolved for ICP-MS analyses (Mori *et al.* 1999). Whole-rock major compositions were obtained using a PANalytical AxiosMAX Advanced spectrometer, following the analytical protocol of Mori *et al.* (1999) and Sertek *et al.* (2015), at the X-Ray Fluorescence Laboratory of Geoanalítica-USP core facility.

PETROGRAPHY

Both TR-IV and LM-I are classified as Group I coherent macrocrystic kimberlites (Cas *et al.* 2008, Le Maitre 2002, Mitchell 1997), with an inequigranular texture (Figs. 2A, 2B) formed by partially-to-fully altered olivine (mega-, macro-, and microcrysts), phlogopite mega- and macrocrysts, and crustal xenoliths set in a very fine groundmass composed mainly of perovskite, olivine, phlogopite, spinel, serpentine, and carbonates. Apatite, ilmenite, and monticellite are also present, but only in LM-I. Garnet macrocrysts and centimetric pyroxene xenocrysts phases are also present in TR-IV and LM-I, respectively (Figs. 2C, 2D). In both intrusions, the mantle xenoliths are peridotites, predominantly dunite or metasomatized harzburgite, with phlogopite, secondary clinopyroxene, chromite, ilmenite, and others. Estimated modal abundances of all the constituent phases are provided in Supplementary Material C.

In TR-IV and LM-I kimberlites, perovskite grains are, in general, similar to the perovskites of group I kimberlites (Chakhmouradian and Mitchell 2000). In both kimberlites, perovskite appears as a major groundmass phase that composes about 5 to 10 vol. % of the rock. The grains are euhedral to subhedral, ranging up to 0.2 mm in size. In LM-I, some perovskite grains show very distinct zoning, occurring as reaction rims in ilmenite. Some small grains are homogeneous, even though many of them show step zoning, with brighter cores and darker rims.

The perovskite crystals were identified in various paragenesis: discrete grains in the groundmass; grains along boundaries of olivine macrocrysts, and macrocrysts forming a "garland" or "necklace" texture (Mitchell 1986; Fig. 2E); complex intergrows with groundmass spinel or titanomagnetite; a reaction rim around Ti-bearing phases like ilmenite macrocrysts (Fig. 2F). All four paragenesis were observed in LM-I. Type (4) is rare in TR-IV. Euhedral inclusions of serpentinized olivine and phlogopite are common in both intrusions. Perovskite is sometimes observed as tiny crystal inclusions within larger poikilitic phlogopite crystals. Those features indicate that perovskite has a protracted crystallization history, allowing the determination of the fO_2 range during the main magmatic evolution of these intrusions.

MINERAL CHEMISTRY

Analyses of major- and minor-element mineral compositions by EPMA are listed in Supplementary Material A for the EPMA data, and analyses of trace-element mineral composition by LA ICP-MS are presented in Supplementary Material B.

Olivine and monticellite

Olivine compositions for TR-IV (Fo_{87-92}) and LM-I (Fo_{83-92}) fall within the compositional range of APAP (Fo_{82-92}, Araújo *et al.* 2001; Fig. 3A) and worldwide (Fo_{84-95}; Mitchell 1986) reported kimberlites. In general, the olivine cores of LM-I present higher NiO and CaO content than those from the TR-IV (Fig. 4).

The NiO, CaO, and Mg# are typically used in the distinction between the mantle and igneous olivine (Bussweiler *et al.* 2015, Foley *et al.* 2013). The "mantle trend" represents typical mantle olivine compositions and it is mainly associated with core analyses, with restricted compositions at relatively high NiO and low CaO concentrations (Bussweiler *et al.* 2015, Foley *et al.* 2013). According to Bussweiler *et al.* (2015), the "melt trend" has been observed in all rim analyses, with the characterization of a decrease in NiO and an increase in CaO concentrations at an almost constant Mg# [Mg/(Mg + Fe), in molecular proportions). However, as the TR-IV and LM-I olivines show extensive serpentinization along crystals rims, the "melt trend" is identified only in a few samples (Fig. 4).

The trace-element contents of olivine are similar to both kimberlites, with Li, Zn and Mn concentrations higher at the olivine rims. The melt trend is enriched in Zr, Ga, Nb, Sc, V, P, Al, Ti, Cr, Ca, and Mn, whereas Zn, Co, Ni and possibly Na are enriched in the mantle trend. The rim and core analysis of both TR-IV and LM-I analyzed olivines results are closely compatible with the described patterns.

Monticellite was only found preserved in the groundmass of LM-I kimberlite. Its Mg# ranges from 72 to 94, indicating a significant compositional variation that is in agreement with literature on APAP kimberlites (74-92; Melluso *et al.* 2008, Araújo *et al.* 2001, Meyer *et al.* 1994, Guarino *et al.* 2013; Fig. 3A). Ca/(Ca + Mg) ratios range between 0.35 and 0.58.

Perovskite

The major and trace element analyses of perovskite samples from TR-IV and LM-I normally indicate a major presence of the ideal $CaTiO_3$ endmember (69–93 mol.% for TR-IV, 86–95 mol.% for LM-I), with contributions of loparite (4–23 mol.% for TR-IV, 2–7 mol.% for LM-I) and $REEFeO_3$ (1–4 mol.% for TR-IV, 2–4 mol.% for LM-I) components (Fig. 3B; calculated following Locock and Mitchell 2018). In general, cores are enriched in REE components, and rims are enriched in the $CaTiO_3$ component.

The highest concentrations of LREE, Nb, and Fe^{3+} (up to 8.8, 4.4 and 5.3 mass% of the respective oxides) are observed

in perovskites from TR-IV samples, which also present higher Sr and Na values (up to 0.86 and 2.8 mass% of the respective oxides) than those from the LM-I. The perovskite trace element compositions of TR-IV and LM-I, which are representative of a single LA-ICP-MS analysis for each crystal due to the large spot-size (providing an average composition of zones of each crystal), are characterized by high concentrations of Sr, Nb, Zr, and REE and show a strong positive correlation between Nb and Ta, Y and Ho, Zr and Nb, Mn and Fe (Fig. 5).

Ilmenite

The macrocrystic ilmenites of LM-I fall into the kimberlitic field, which agrees with literature data from other APIP kimberlites (Guarino *et al.* 2013); however, it is characterized by higher MgO at a given TiO_2. There is also a large variation in Cr_2O_3. Based on these variations, Golubkova *et al.* (2013) divided Mg-ilmenites from kimberlites into three different groups and showed three different zoning patterns (trends) that define a characteristic parabolic curve (Fig. 6). The first

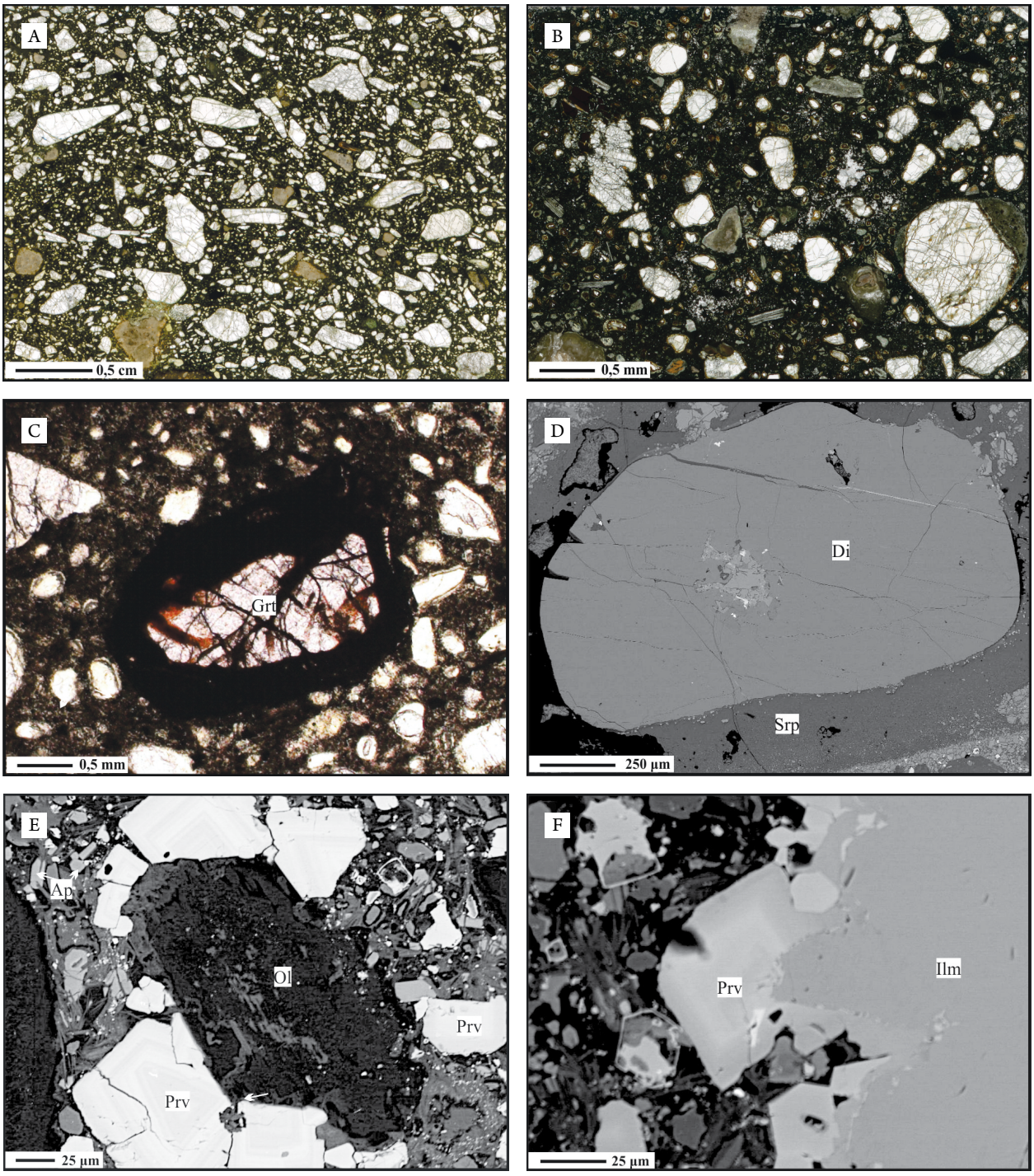

Figure 2. Petrographic aspects of TR-IV and LM-I kimberlites. General view of inequigranular macrocrystic texture of (A) TR-IV and (B) LM-I kimberlites. (C) TR-IV garnet xenocryst with a keliphitic rim (plane-polarized transmitted light). (D) LM-I pyroxene xenocryst with serpentine rim (BSE image). BSE images showing petrographic aspects of perovskites: (E) zoned perovskite crystals as "garland" or "necklace" textures in olivine (LM-I); (F) perovskite as a reaction rim around an ilmenite crystal (LM-I).

two trends are observed in LM-I ilmenites. Trend 1 is characterized by reversed zoning patterns with an increase in MgO towards the rims. An increase in the MnO content is also observed towards the rims around 0.7 mass%. Trend 2 is characterized by an increase in MgO and a decrease in Cr_2O_3 content towards the rims in some Mg-ilmenite grains. In terms of MgO and Cr_2O_3 concentration, this trend corresponds to the left side of the parabolic curve in the binary diagram. The third type of zoning patterns (Trend 3) presents a significant drop in MgO and Cr_2O_3 and an increase in MnO content, which is not observable in LM-I Mg-ilmenites compositions.

Clinopyroxene

Clinopyroxene xenocrysts from LM-I (mantled by a reaction zone with serpentine and monticellite) and microcrysts in the groundmass of TR-IV (associated with reaction zones of crustal xenoliths) plot in the diopside-hedenbergite field in the Es-Wo-Fs diagram (Fig. 3C). Clinopyroxenes from all the samples vary in CaO, Na_2O, and Cr_2O_3 content. Xenocrystic clinopyroxene from LM-I presents higher MgO and FeO concentration than microcystic clinopyroxenes from TR-IV.

Garnet

All the garnet samples are identified as pyrope (62 to 73 mol.%) with Cr_2O_3 contents between 0.67 and 7.20 mass%, and CaO contents between 3.99 and 5.67 mass%. TiO_2 is generally low, and Mg# values are variable (72 to 79 mol.%). According to the garnet classification scheme of Grütter *et al.* (2004), the TR-IV studied samples can be identified as lherzolitic (G9) and pyroxenitic (G4, G5), as seen in Fig. 3D.

BULK ROCK COMPOSITIONS

Major element concentrations of TR-IV and LM-I kimberlites are reported in Supplementary Material D. Both LM-I and TR-IV kimberlites are ultrabasic, silica-undersaturated, Al-poor (Al2O3 < 5 wt.%), with high LOI (largely due to the abundant presence of volatile-bearing phases, such as carbonates, serpentine and phlogopite)

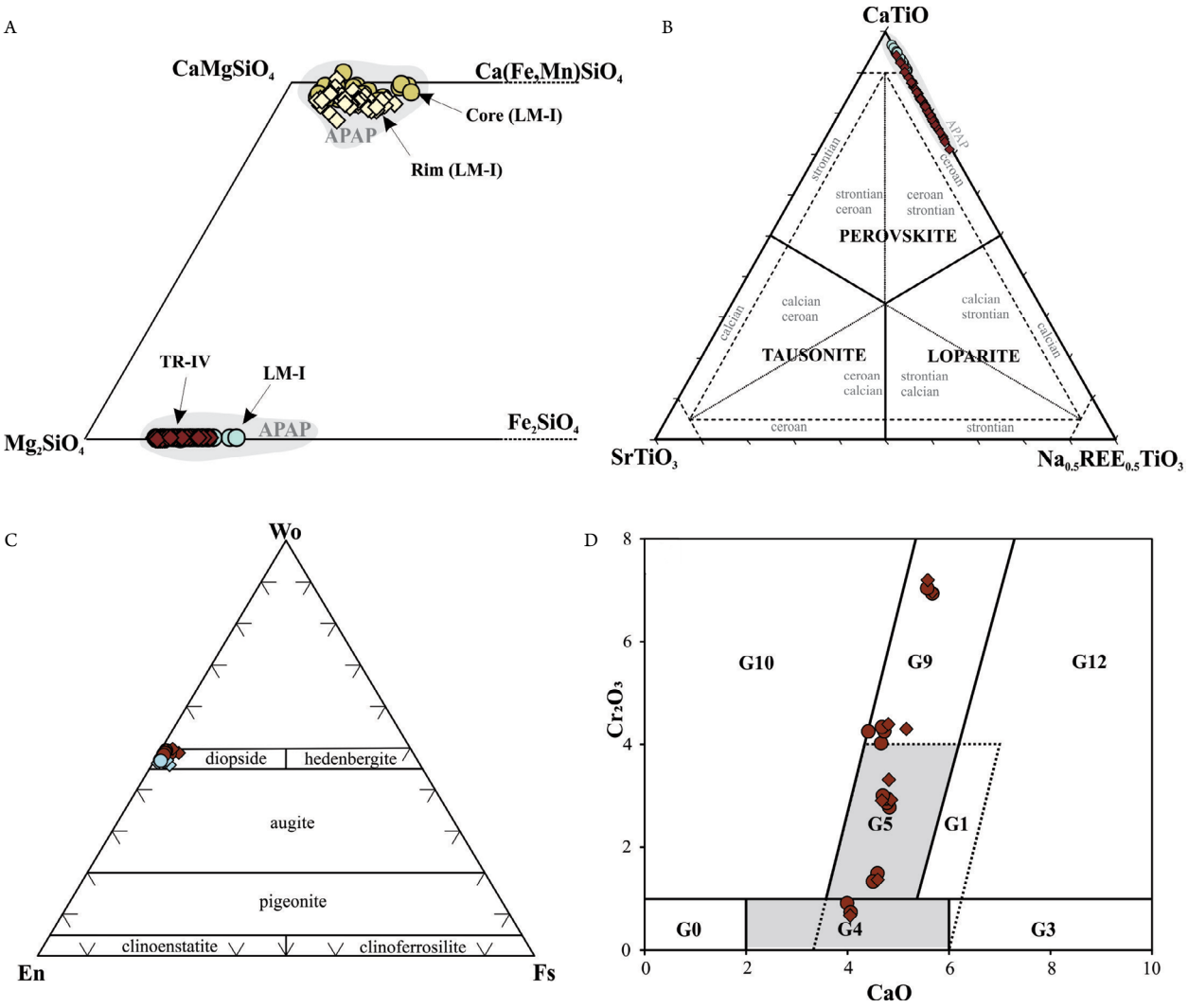

Figure 3. Mineral compositions of LM-I and TR-IV kimberlites. (A) Olivine diagram. (B) Perovskite composition plotted in the tausonite-perovskite-loparite ternary system (Locock and Mitchell 2018). (C) Classification diagram of clinopyroxenes. (D) Pyrope analyses plotted in the G-number nomenclature classification scheme (after Grütter *et al.* 2004). Symbols – light blue: LM-I brown: TR-IV; diamond: crystal rim; circle: crystal core. Grey fields are APAP literature data compiled from Meyer *et al.* (1994), Araújo *et al.* (2001), Melluso *et al.* (2008), Guarino *et al.* (2013), Felgate (2014).

and high Mg# [MgO/(MgO + FeO_T), in mol. proportion]. Overall, those rocks are CaO-rich, Al_2O_3– and Na_2O-poor, as well as potassic in character (K_2O = 0.9–1.6 mass% and 0.7–1.2 mass% for LM-I and TR-IV respectively). All major element contents are within the intervals known from the literature data based on the APAP kimberlites (SiO_2 = 25.3–34.2 mass%; MgO = 20.2–32.7 mass%; Mg# 60–86; CaO = 6.5–15.4 mass%; Al_2O_3 = 4–3–3 mass%; Na_2O = 0.02–1.4 mass%; K_2O = 0.54–3 mass%; Bizzi *et al.* 1994, Meyer *et al.* 1994, Gibson *et al.* 1995a, Carlson *et al.* 1996, Melluso *et al.* 2008, Felgate 2014). The Fe_2O_3 range for LM-I (10.93–11.06 wt.%) is a little higher than that found for the TR-IV (9.21–9.44 wt.%). For whole-rock trace element and isotopic compositions of LM-I and TR-IV kimberlites, the reader is referred to Carlson *et al.* (1996), Gibson *et al.* (1995a,b) and Melluso *et al.* (2008).

QUANTIFICATION OF INTENSIVE PARAMETERS

P-T conditions

Due to the presence of distinct paragenesis in LM-I and TR-IV kimberlites, different geothermobarometers were tested: enstatite-in-clinopyroxene, Al-in-olivine, chromium-in-pyrope, and Ni-in-garnet.

For the LM-I, the geothermometer of Nimis and Taylor (2000), based on enstatite-in-cpx, was applied to its diopside xenocrysts, following the compositional recommendations of Nimis and Grütter (2010) for a safer selection of clinopyroxenes. The calculated temperature ranges from 718 to 986°C, using a constant pressure of 40 Kbar, which is an average pressure value reported in literature for several APAP kimberlites. The uncertainties related to that geothermometer are considered

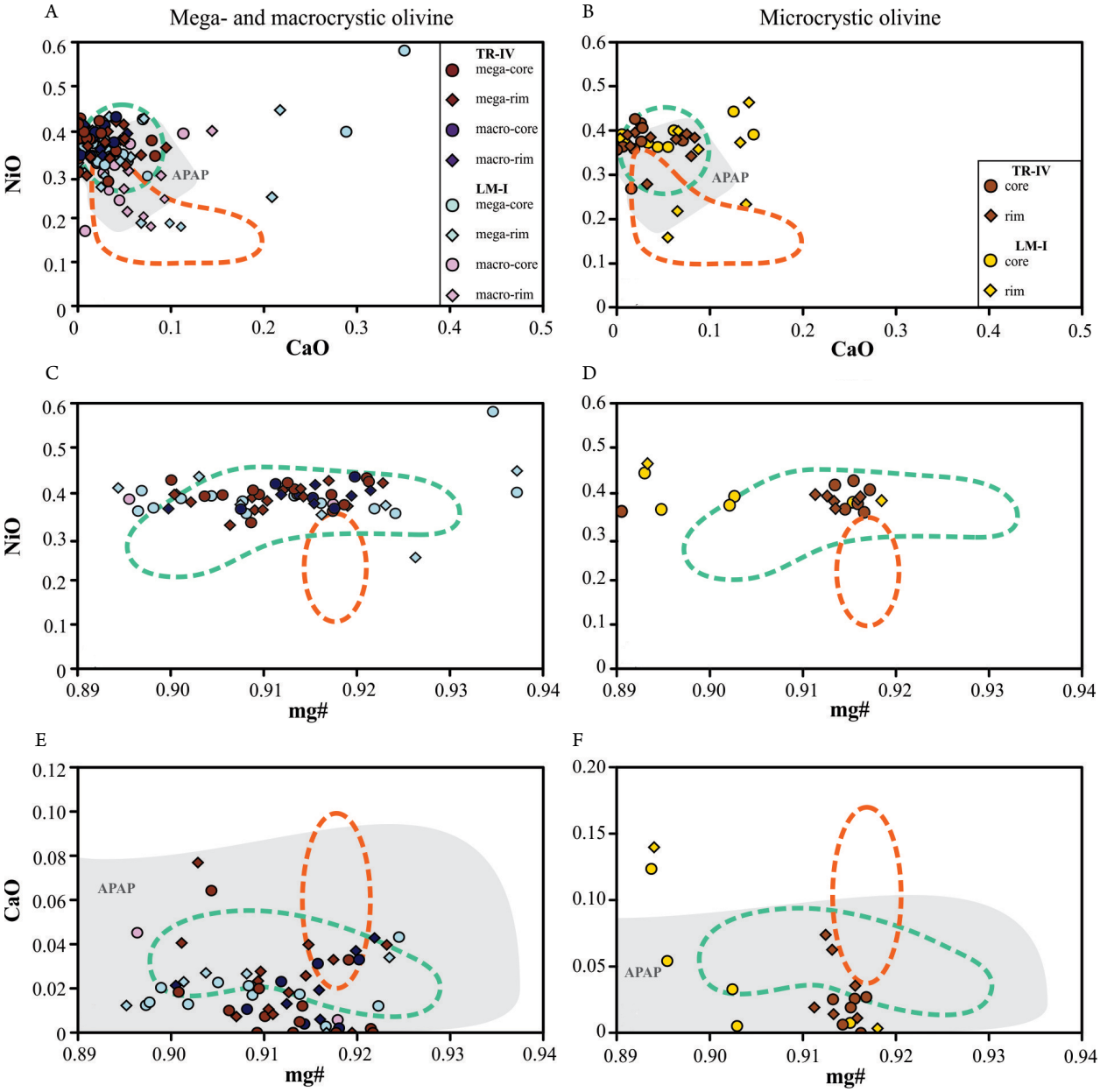

Figure 4. Variation diagrams for mega- macro- and microcrystic olivine; Mantle trend (green) and melt trend (orange) fields are from Bussweiler *et al.* (2015) and were determinate according to South African kimberlites compositions. Grey fields represent APAP literature data compiled from Meyer *et al.* (1994), Araújo *et al.* (2001) and Melluso *et al.* (2008).

equivalent, or most of the widely used thermobarometers for garnet peridotites (Nimis and Taylor 2000). The LM-I clinopyroxene xenocrysts analyzed in this paper are identified as garnet-facies clinopyroxene, which can be interpreted as mantle xenocrysts derived from disaggregated garnet-facies lherzolite xenoliths (Read *et al.* 2004, Fig. 7A). Read *et al.* (2004) proposed a single empirical curve for all APAP garnet-facies clinopyroxene that falls within a 600 to 1,000°C temperature range, which represents the lithospheric geotherm at the kimberlite eruption (37-mW/m²). Based on the calculated temperature, an estimation of pressure with such geotherm empirical curve resulted in a variation from 37 to 47 Kbar for clinopyroxene from the LM-I kimberlite. Another approach to temperature calculations is the Bussweiler *et al.* (2017) Al-in-olivine thermometer for mantle peridotites. This version of the Al-in-olivine thermometer is applicable to garnet peridotites (lherzolites and harzburgites), but not to spinel-bearing peridotites (Bussweiler *et al.* 2017). Some olivine cores from the LM-I fall within the garnet peridotite field (high Al and high V, Fig. 7B), which was used in the Al-in-olivine thermometer with a constant pressure of 47 Kbar and calculated with the empirical geotherm curve of Read *et al.* (2004). The application of this geothermometer resulted in a temperature range from 985 ± 13°C. The 2σ error presented in the Ni content has been considered.

For the TR-IV kimberlite, chromium-in-pyrope geobarometer of Grütter *et al.* (2006) was applied for their pyrope xenocrysts

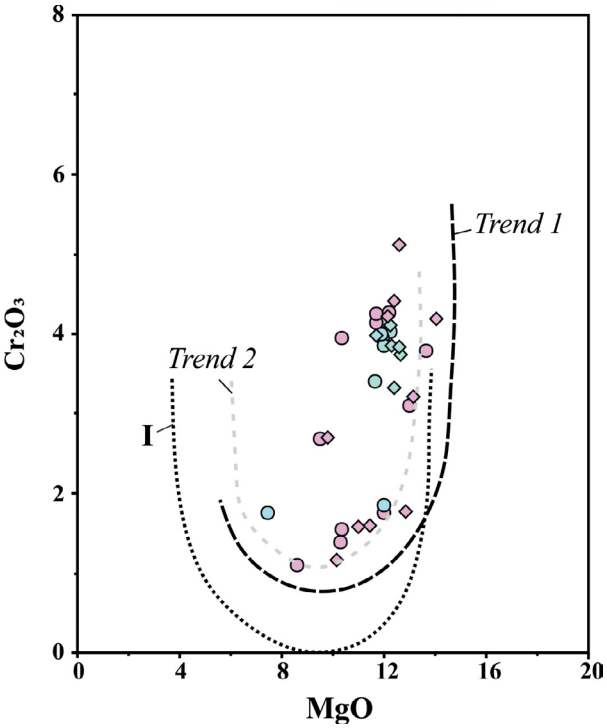

Figure 6. Variation of MgO *versus* Cr_2O_3 concentrations on LM-I and TR-IV ilmenites. Dashed "parabolic" curves represent I - "typical" Mg and Cr distribution in ilmenite megacrysts from kimberlites after Haggerty (1983); Trends 1 and 2: curves defined by Golubkova *et al.* (2013) for Mg-ilmenites from kimberlites.

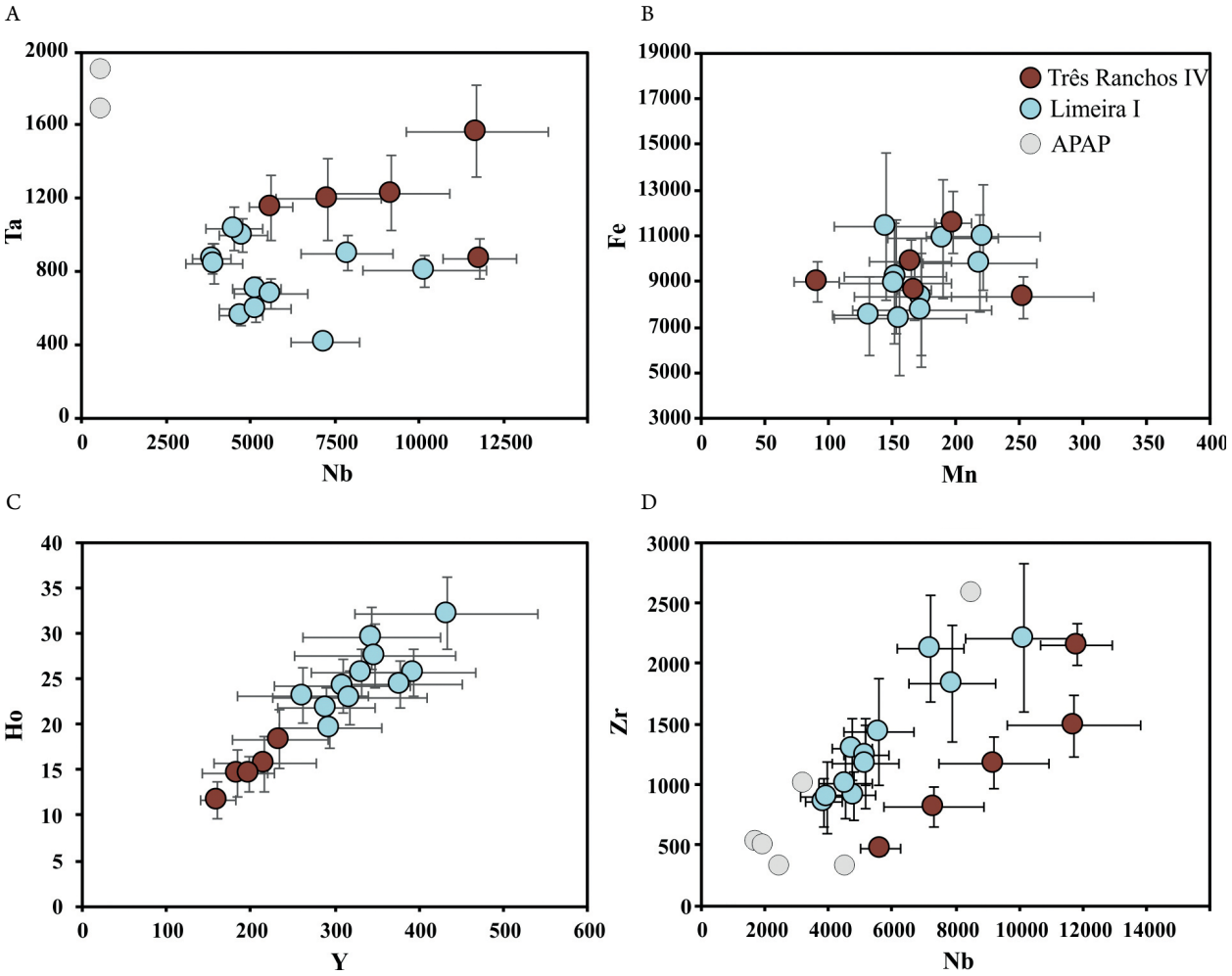

Figure 5. Compositional variations of major and trace elements in perovskites from TR-IV and LM-I.

and yields pressures that range from 18 to 34 Kbar. With the same barometer, an estimation using the available chemical data (Cabral Neto *et al.* 2017) in garnets from other APAP kimberlites resulted in 18 to 42 Kbar. Ni-in-garnet geothermometers (Canil 1999), which use partitioning of Ni between olivine and garnet, were applied to a sample of TR-IV kimberlite using a constant pressure of 34 Kbar. This partition is temperature-dependent and can constitute a useful geothermometer in the interpretation of mantle-derived garnets (Canil 1999). With this thermometer, calculations for TR-IV yield a temperature range from 975 ± 19 to 1,050 ± 24°C. Some olivine cores from TR-IV present the chemical characteristics of a garnet peridotite (Fig. 7A). The Al-in-olivine thermometer (Bussweiler *et al.* 2017) under constant pressure of 36 Kbar (estimated from garnet composition of the same rock sample) yielded a temperature of 1,270 ± 13°C (considering analytic aluminum 2σ error).

Oxygen fugacity

Several studies have used the composition of perovskite to estimate fO_2 through Nb and Fe content (Fedortchouk and Canil 2004). Bellis and Canil (2007) calibrated the compositional variation of perovskite experimentally as an oxygen barometer, applying an empirical relation (Equation 1) to describe the covariation of Fe and Nb cations in the mineral with fO_2 related to the NNO variation (uncertainties at 2σ, besides Nb and Fe as cations by three oxygens):

$$\Delta NNO = \frac{\left[0.50(\pm 0.021)\,x\,Nb - Fe(\pm 0.031) + 0.030(\pm 0.001)\right]}{0.004(\pm 0.0002)} \quad (1)$$

The variation in nickel-nickel oxide buffer (ΔNNO, fO_2 related to that of the Nickel-bunsenite NNO buffer) was calculated for the perovskites of LM-I and TR-IV, both presenting wide intervals that are similar to other kimberlites of the literature (Canil and Bellis 2007; Fig. 8A). Perovskite crystals from LM-I (Fig. 8B) indicate ΔNNO, ranging from -3.2 to +2.1, with an average value of -1.3 and standard deviation of ± 1.4 (n = 81). Perovskite crystals from TR-IV (Fig. 8B) indicate ΔNNO ranging from -5.9 to +2.5, with an average value of -2.4 and a standard deviation of ±1.3 (n = 120).

Another oxygen fugacity calculation procedure involves the estimation of Fe composition in kimberlite liquid and monticellite. Studies by Le Pioufle and Canil (2012) demonstrated the use of an oxybarometer for kimberlite magmas, based on

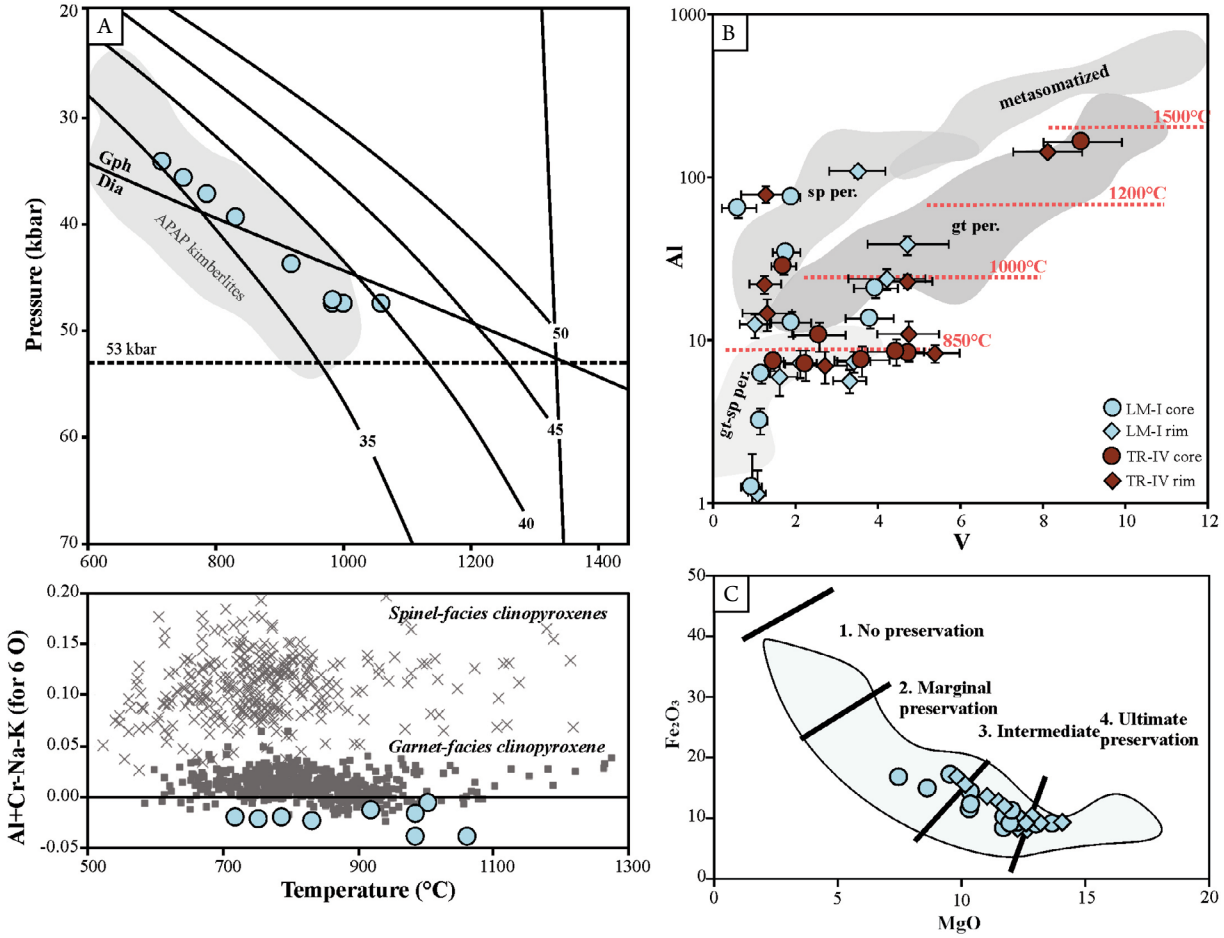

Figure 7. (A) P-T conditions and compositions for LM-I clinopyroxenes. The grey field for the APAP kimberlites and clinopyroxene samples (garnet-facies: grey squares; spinel-facies: grey crosses) are compiled from Read *et al.* (2004); (B) Al *versus* V concentration of olivine rims and cores from TR-IV and LM-I (bars represent 2σ error/uncertainties for the analyzed olivine). Grey fields represent compositional variations of different mantle facies (based on data by Bussweiler *et al.* 2017); (C) FeO *versus* MgO discrimination diagram for the LM-I ilmenite samples. Fields proposed by Gurney and Zweistra (1995) define the diamond preservation grade in kimberlite from the composition of its ilmenite xenocrysts.

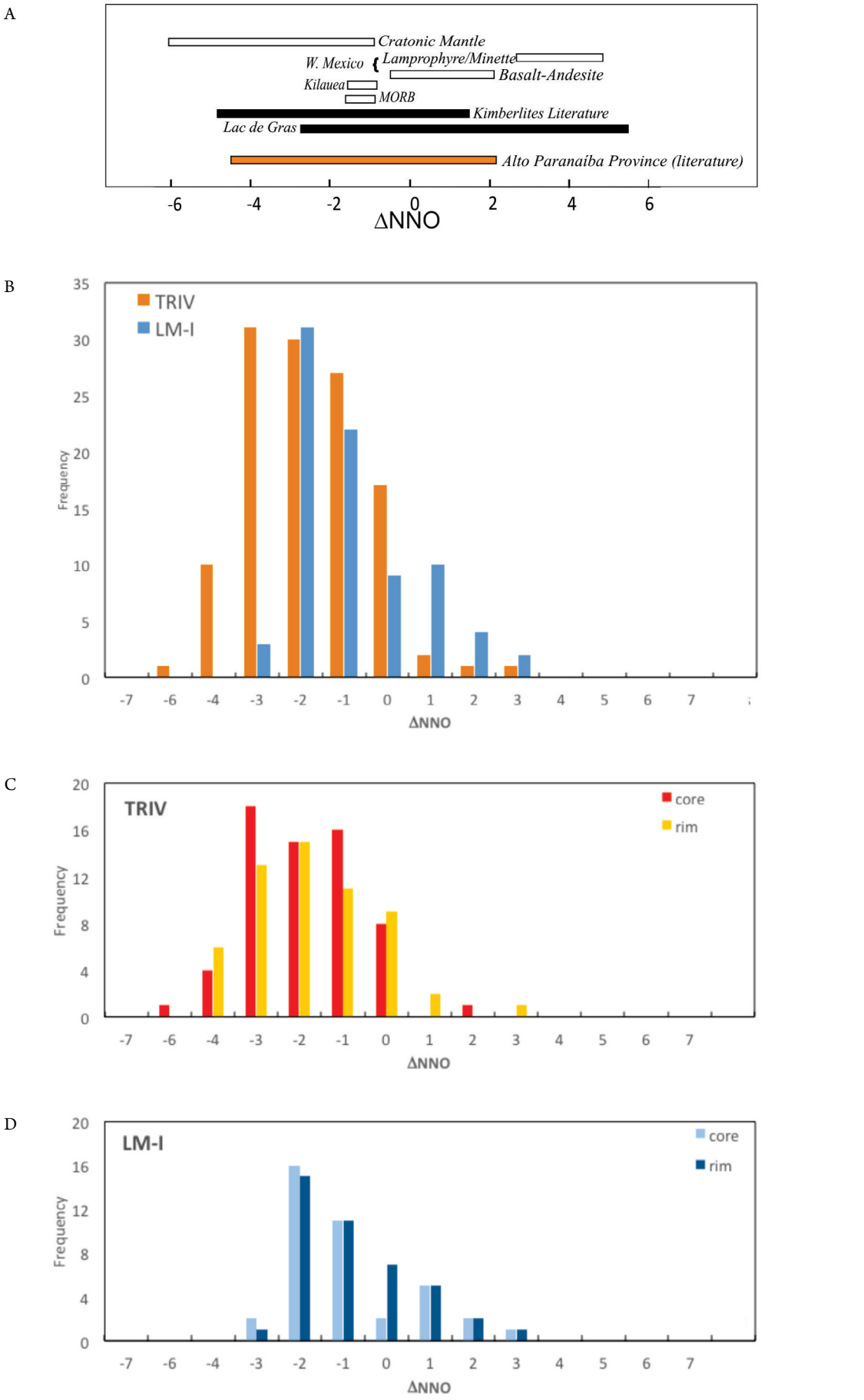

Figure 8. Oxygen fugacity variation in function of ΔNNO (calculated based on the composition of perovskite according to Bellis and Canil 2007). (A) fO_2 intervals for global kimberlite bodies and other mantle-derived magmas (from Canil and Bellis 2007) and for previously published perovskite data of Alto Paranaíba Alkaline Province (Meyer *et al.* 1994, Araújo *et al.* 2001, Melluso *et al.* 2008, Felgate 2014). (B) Histogram of fO_2 calculated values (in terms of ΔNNO) for TR-IV and LM-I intrusions. (C, D) Histogram of fO_2 calculated values (in terms of ΔNNO) for TR-IV and LM-I, respectively, contrasting the values obtained from core and rim compositions.

the amount of Fe in monticellite ($CaMgSiO_4$) in equilibrium with kimberlite liquids in experiments at 100 kPa, with temperatures varying from 1,230 to 1,350°C and log fO_2 from NNO -4.1 to NNO +5.3. The equation proposed for this oxybarometer (Equation 2) is:

$$\Delta NNO = \frac{\left\{ log\left[0.858(\pm 0.021)\frac{X_{Fe}^{Liq}}{X_{Fe}^{Mtc}} - 1 \right] - 0.139(\pm 0.022) \right\}}{0.193(\pm 0.004)} \quad (2)$$

In which XFe_{Liq} and XFe_{Mtc} correspond to the molar fraction of Fe in the liquid and monticellite, respectively (Le Pioufle and Canil 2012). The global analysis of the matrix of such samples may be considered a good approximation of such liquid, since many xenocrysts are carried by kimberlitic magmas. This oxybarometer was applied only to LM-I kimberlite, once monticellite was not found in the TR-IV, which had been probably replaced with serpentine. All bulk compositions were recalculated on a volatile-free basis. XFe_{Liq} was determined for three LM-I samples from bulk composition data. An average value was therefore applied to different samples of the same pipe.

The Fe present in the "liquid" composition was calculated based on whole-rock compositions and without including the amount of the main xenocrysts. The amount of olivine (with less than 5% considered to have crystallized from the magma itself, Brett *et al.* 2009) and phlogopite macrocrysts was interpreted as the main xenocrysts in these rocks (Supplementary Material C). Ubide *et al.* (2012) suggest Equation 3 to yield quantitative proof that the proportions of each member (groundmass and mega-, macrocrysts) reflect its proportions in the rock:

$$C_{WR}^{i} = C_{Mt}^{i}\left(1 - \sum \nu\right) + \sum\left(C_{Mg}^{i} x\, \nu\right) \quad (3)$$

In which:
C_{WR}^{i}, C_{Mt}^{i}, C_{Mg}^{i} = the concentrations of an *i* element in the whole rock composition (WR), in both matrix (Mt) and mega-, macrocrysts (Mg), respectively;
ν = the modal volume of the mega-, macrocrysts of olivine and phlogopite.

Likewise, the following equation was applied to the studied kimberlites (Equation 4):

$$C_{Mt}^{i} = \frac{C_{WR}^{i} - C_{Phl}^{i} x\, \nu_{Phl} - C_{ol}^{i} x\, \nu_{ol}}{1 - \nu_{Phl} - \nu_{ol}} \quad (4)$$

All elements were then recalculated on an anhydrous basis (C_{Mt}^{i} mass% / sum. x100). The calculated liquid compositions are also presented in Supplementary Material D. For LM-I, XFe_{Mtc} ranges from 0.020 to 0.087. The average of XFe_{Liq} is 0.120 (Fig. 9). The same molar fractions were calculated based on APAP monticellite data reported in literature, with XFe_{Mtc} and XFe_{Liq} ranging from 0.022 to 0.077 and from 0.090 to 0.184, respectively. The fO_2 for LM-I monticellite calculated using Equation 3 varies from -4.2 to +2.5 ΔNNO, with a ΔNNO average of -0.1 and standard deviation of 1.74 (n = 84). As calculated from compilation of previous APAP data, it varies from NNO -4.50 to +2.60.

DISCUSSION

Crystallization interval for Alto Paranaíba kimberlites

P-T data acquired from LM-I samples show that even though the kimberlite is known to be barren, the garnet-lherzolite facies clinopyroxene and olivine xenocrysts analyzed in this study indicate that the magma could have at least crossed the diamond stability field (Fig. 7A). Mg-ilmenite, which is an important indicator used in diamond exploration, is also present as xenocrystic phases in the LM-I samples (Fig. 7C). On the other hand, garnet data from samples of the diamond-bearing TR-IV kimberlite in this study indicate much lower pressure than the ones from the diamond stability field. However, the Cr-in-pyrope barometer is related to a minimum pressure estimate for such xenocrysts. Therefore, it does not rule out the relationship with the diamond field. These specific sampled xenocrysts may have been formed at shallower horizons, so the comparison of pressure and temperature in TR-IV and LM-I and their relation

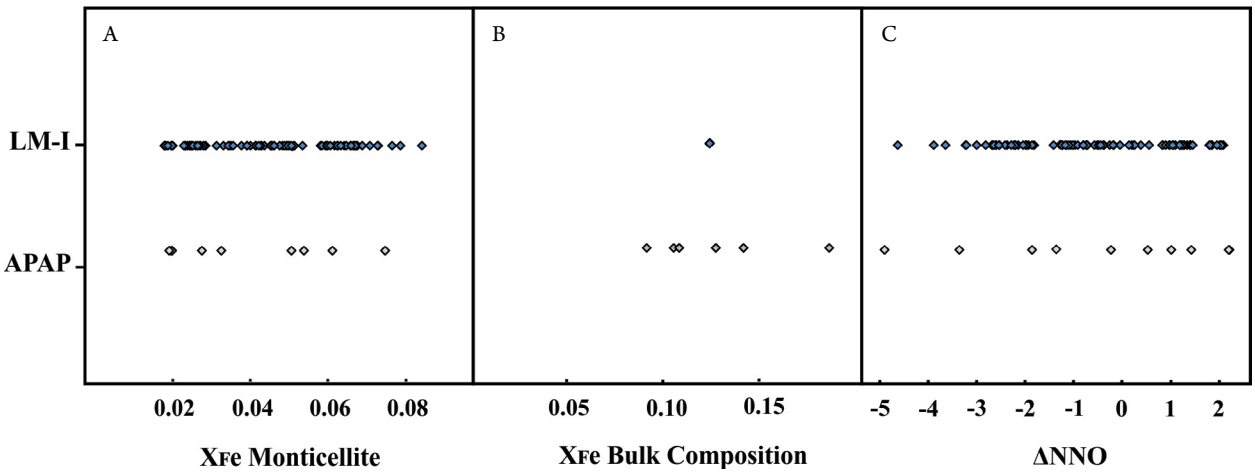

Figure 9. XFe of monticellite and bulk kimberlite "liquid" composition, and ΔNNO estimates for LM-I kimberlite. (A) XFe of monticellite expressed as molar fraction. (B) XFe of the bulk composition expressed as molar fraction. (C) ΔNNO calculated with Equation 3 for LM-I and other kimberlites from APAP (calculated using mineral chemical data from Melluso *et al.* 2008, Meyer *et al.* 1994, Guarino *et al.* 2013).

to diamond stability in these magmas is inconclusive. It is known that besides P-T conditions, diamond stability is also dependent on oxygen fugacity, and this parameter may affect the properties, textures and preservation of diamonds in the kimberlite magma (Bellis and Canil 2007, Nowicki *et al.* 2007).

During the crystallization history of kimberlite magmas, the fO_2 can vary significantly from initial to late stages, as indicated by the perovskite compositions in occurrences worldwide (Bellis and Canil 2007, Canil and Bellis 2007, Sarkar *et al.* 2013). Perovskite crystallization follows most macrocrystic phases, such as olivine and Cr-spinel (Clement 1982, Mitchell 1986, 2008, Chakhmouradian and Mitchell 2000, Sarkar *et al.* 2013), but it may also coexist with Fe-Ti spinel and magnetite, which suggests simultaneous crystallization. This cognate phase becomes very unstable during the final magma evolution stages, when there is excessive CO_2 in the system (Mitchell and Chakhmouradian 1998). This leads to the reaction of perovskite with the CO_2-rich fluid, forming a TiO_2 polymorph (rutile) and calcite that could precipitate in the perovskite vicinities, giving the grains a spongy appearance (Sarkar *et al.* 2013).

In our study case, most of the TR-IV and LM-I perovskite crystals occur as a discrete groundmass phase and appear to have remained very fresh and not converted into rutile. Thus, a reaction with a CO_2 fluid may not have taken place. Considering uncertainties, there is an important superposition of fO_2 values between the two intrusions, with a tendency for more reduced conditions for TR-IV. The core-to-rim fO_2 variations are very low and present trends towards more reduced conditions for some crystals, while trends towards more oxidized conditions were also found in similar proportions. Therefore, both oxidation and reduction tendencies can occur during the crystallization of each intrusion. In general, the fO_2 ranges calculated for the core compositions are very similar to the ranges calculated for the rim compositions of each intrusion (Fig. 8C, 8D). This variability in the oxygen fugacity values can be caused by several processes, such as degassing, decompression (Carmichael and Ghiorso 1986, Sparks *et al.* 2006), crystallization (Carmichael and Nicholls 1967), and magma mixing (Sarkar *et al.* 2013). Both fO_2 ranges are within the variation found for previously published perovskite values for other kimberlites from APAP (Melluso *et al.* 2008, Felgate 2014, Araújo *et al.* 2001, Meyer *et al.* 1994) and worldwide (Bellis and Canil 2007, Trickett 2007), as seen in Fig. 8.

The perovskite oxybarometer from Bellis and Canil (2007) yields fO_2 values that range from -3.2 to +2.1 ΔNNO for LM-I kimberlite, while the monticellite oxybarometer of Le Pioufle and Canil (2012) yields fO_2 values that range from -4.2 to +2.5 ΔNNO for the same intrusion. This comparison was not possible for the TR-IV, considering the possible monticellites were completely altered in the groundmass. This represents the monticellite oxybarometer first limitation, because this mineral may be altered and replaced with serpentine in kimberlite intrusions. Calibration of the perovskite oxybarometer bears a large uncertainty of ± 1 log fO_2 unit (Bellis and Canil 2007), but it has the potential advantage of being applicable to distinct evolution stages of kimberlite magmas, which are recognized by their different perovskite compositional types in kimberlite intrusions (Canil and Bellis 2007).

Possible associations between oxygen fugacity and diamond instability

It is widely recognized that many diamonds are partially reabsorbed during the ascent of magma from the upper mantle to the Earth's surface, mostly by oxidation (Robinson 1979). This is a common process. Many diamonds exhibit the rounded dodecahedral morphology from their original octahedral shapes (Nowicki *et al.* 2007), under which oxidation is considered likely to cause many microdiamonds (> 0.5 mm) to be completely resorbed. High-temperature kimberlitic melts are very reactive with the crust environment (Malarkey *et al.* 2010), and this may possibly be the cause of diamond resorption.

Considering that co-crystallization of olivine-spinel occurs below 1.0 GPa, the maximum oxygen fugacity values of kimberlitic magmas (in a silica-buffered activity and diopside-monticellite) are in the graphite stability field, *i.e.* very close to the D/GCO (Diamond/Graphite and CO_2) buffer (Fedortchouk and Canil 2004). With increasing pressure, fO_2 values reach the CO_2 stability field. Thereby, any diamond released from depth xenoliths will have undergone dissolution in the graphite stability field, while those in contact with the magma in the final stages of eruption are possibly reabsorbed in the CO_2 stability field (Fedortchouk and Canil 2004). Although the diamond preservation degree is probably a result of the amount of these crystals in the mantle by ascending kimberlitic magma, the kimberlites fO_2 are estimated to be of some utility in predicting the quality or properties of such diamonds (Fedortchouk and Canil 2004). Kimberlite pipes with higher oxygen fugacity display the largest proportions of strongly absorbed diamonds, while pipes with lower fO_2 values present lower degrees of diamond absorption (Canil and Bellis 2007). This suggests that oxygen fugacity affects the properties and textures of the diamonds preserved in the magma (Canil and Bellis 2007).

Studies have demonstrated that all reabsorbed natural diamonds undergo powerful condition-controlled dissolution, which overwhelms the effects of internal factors on diamond resorption (Fedortchouk *et al.* 2005, Fedortchouk and Canil 2009, Zhang 2016). In the lithospheric mantle, diamonds are stable at T = 900–1,400°C, P = 4 to 7 GPa, and fO_2 at NNO between -5 and -1 (Stagno *et al.* 2013, Stachel and Luth 2015). Kimberlites are believed to be formed at 1,450°C (Kavanagh and Sparks 2009), and their average crystallization T is ~ 1,030°C estimated through olivine-spinel thermometry (Fedortchouk and Canil 2004). The fO_2 of TR-IV constrained by perovskite (kimberlite cognate phase) oxygen barometry presents an average value of -2.4 for ΔNNO, with standard deviation of ± 1.30 (n = 120), whereas those calculations for LM-I have an average value of -1.31 for ΔNNO, with standard deviation of ± 1.38 (n = 81). Considering these uncertainties, there is an important superposition of fO_2 values between both intrusions, with a possible tendency for more reduced conditions for TR-IV (Fig. 8).

Although perovskite and monticellite data are available for several Brazilian kimberlite intrusions (*e.g.*, Indaiá, Limeira, Pântano, Três Ranchos — Araújo *et al.* 2001, Melluso *et al.* 2008, Felgate 2014), only TR-IV is reported as a diamond-bearing kimberlite. When compared to other diamond-bearing kimberlites

worldwide, TR-IV shows a fairly large range of ΔNNO, which is similar to that obtained for the diamond-bearing Orapa kimberlite, Botswana (ΔNNO from -5.5 to ~1, Sarkar *et al.* 2013). Orapa fO_2 values show a tendency for more reduced conditions, which is equal to that suggested for TR-IV. However, it is noteworthy that the barren kimberlites from APAP (Fig. 8) display fO_2 conditions mostly within the range of diamond-bearing kimberlites from Lac de Gras area, Canada (ΔNNO from -4 to +6; Canil and Bellis 2007). Due to the superposition of ranges and absence of a preferential trend, we consider the influence of fO_2 uncertain for the possible instability of diamonds on APAP. During the crystallization history of kimberlite magmas, it is difficult to assign only a single intrinsic parameter to the diamond grade of preservation or even its dissolution. A combination of intensive parameters during the crystallization of kimberlite magmas may also have some effect on the preservation grade of the diamond or on its dissolution: the fO_2 and P-T variations during the final stages of crystallization, the degree and speed of undercooling, the action of fluids, and the ascent rate (Zhang 2016). In some cases, in which diamond-bearing kimberlite occurrences experienced high amounts of CO_2 degassing, such as Premier pipe (South Africa), groundmass mineral oxybarometry may have little value for the diamond prediction (Dongre and Tappe 2019). This does not seem to be the case for APAP occurrences. However, as highlighted by Talukdar and Chalapathi Rao (2015), only a combined approach (detailed petrography, geochemistry and oxybarometry) on individual intrusions may provide reliable predictions regarding the presence of diamonds in kimberlites, considering the uncertainties.

CONCLUSIONS

Two kimberlite intrusions (diamond-bearing TR-IV and barren LM-I) in the APAP were discriminated based on P-T-fO_2 conditions, the main mineral phases chemistry and bulk rock geochemistry. Several geothermobarometers applied for rocks of these intrusions, as well as the compositional trends found for mantle xenocrysts, indicated that both intrusions crossed the mantle garnet-facies, and potentially the conditions of the diamond stability field. The TR-IV fO_2 constrained by perovskite (kimberlite cognate phase) oxygen barometry presents an average value of -2.4 for ΔNNO, with standard deviation of ± 1.30 (n = 120), whereas those calculations for LM-I have an average value of -1.31 for ΔNNO, with standard deviation of ± 1.38 (n = 81). Considering these uncertainties, there is an important superposition of fO_2 values between both intrusions, with a tendency for more reduced conditions for TR-IV. For the LM-I intrusion, an oxybarometer based on the composition of monticellite, a cognate late-stage phase in kimberlites, yielded a value range between -4.2 and +2.5 for ΔNNO, which is congruent with the range calculated from the perovskite compositions (ΔNNO: -3.2 to +2.1). Due to the superposition of ranges and absence of a preferential fO_2 trend between the two intrusions, we consider the influence of fO_2 uncertain for the possible instability of diamonds. This study only represents a first approach in this theme, trying to evaluate an additional variable in the discussion of the APAP economic potentiality.

ACKNOWLEDGMENTS

This research study was granted by *Fundação de Amparo à Pesquisa do Estado de São Paulo* — FAPESP (processes 2016/12627-6, BC; 2012/06082-6, 2017/03768-8, RGA, ER; 2018/15731-4, LC). RGA acknowledges a productivity grant from *Conselho Nacional de Desenvolvimento Científico e Tecnológico* — CNPq (304148/2017-2). MSc. Nicholas Machado Lima and MSc. Júlio César Lopes da Silva are acknowledged by the important help in the fieldwork in the APAP for the sample collection. We also thank the analytical support of the technicians from the laboratories of GeoAnalítica-USP facilities. The authors appreciated and acknowledge the helpful comments and suggestions of Dr. Y. Weiss and Dr. S. Valente, and the editorial support of Cláudio Riccomini, who improved an early version of the manuscript.

ARTICLE INFORMATION

Manuscript ID: 20190087. Received on: 09/04/2019. Approved on: 12/17/2019.

B.C. developed her master's dissertation on this topic and wrote a first draft of the manuscript; R.A. advised B.C. on her master's and wrote some parts of the final manuscript; L.C. wrote some parts of the final manuscript and helped with the discussions; E.R. and D.S. helped in geological controls and sampling of the studied intrusions and participated in the discussions for the paper.

Competing interests: The authors declare no competing interests.

REFERENCES

Almeida F.F.M. 1983. Relações tectônicas das rochas alcalinas mesozóicas da região meridional da plataforma sul-americana. *Revista Brasileira de Geociências*, **13**(3):39-158.

Almeida V.V. 2009. *Mineralogia e Petrologia de Xenólitos Mantélicos das Regiões de Ubatuba (SP) e Monte Carmelo (MG): Evidências de Fusão Parcial e Metassomatismo no Manto Superior do Sudeste do Brasil*. MS Dissertation, Instituto de Geociências, Universidade de São Paulo, São Paulo, 112 p.

Andrade S., Ulbrich H.H., Gomes C.B., Martins L. 2014. Methodology for the determination of trace and minor elements in minerals and fused rock glasses with laser ablation associated with quadrupole inductively coupled plasma mass spectrometry (LA-Q-ICP-MS). *American Journal of Analytical Chemistry*, **5**(11):701-721. http://doi.org/10.4236/ajac.2014.511079

Araújo A.L.N., Carlson R.W., Gaspar J.C., Bizzi L.A. 2001. Petrology of kamafugites and kimberlites from the Alto Paranaíba Alkaline Province, Minas Gerais, Brazil. *Contributions to Mineralogy and Petrology*, **142**:163-177. https://doi.org/10.1007/s004100100280

Armstrong J.T. 1995. Citzaf-a package of correction programs for the quantitative Electron Microbeam X-Ray-Analysis of thick polished materials, thin-films, and particles. *Microbeam Analysis*, **4**:177-200.

Ballhaus C., Frost B.R. 1994. The generation of oxidized CO_2-bearing basaltic melts from reduced CH4-bearing upper mantle source. *Geochimica et Cosmochimica Acta*, **58**(22):4931-4940. https://doi.org/10.1016/0016-7037(94)90222-4

Bellis A., Canil D. 2007. Ferric iron in $CaTiO_3$ perovskite as an oxygen barometer for kimberlitic magmas I: experimental calibration. *Journal of Petrology*, **48**(2):219-230. https://doi.org/10.1093/petrology/egl054

Biondi J.C. 2005. Brazilian mineral deposits associated with alkaline and alkaline-carbonatite complexes. *In*: Comin-Chiaramonti P., Gomes C.B. (Eds.). *Mesozoic to Cenozoic Alkaline Magmatism in the Brazilian Platform.* São Paulo: FAPESP, p. 707-750.

Bizzi L.A., Smith C.B., Wit M.J., Armstrong R.A.A., Meyer H.O.A. 1994. Mesozoic kimberlites and related alkalic rocks in south-western São Francisco Craton, Brazil: a case for local mantle reservoirs and their interaction. *In*: International Kimberlite Conference, 5., Araxá. *Annals…*, p. 156-171.

Brett R.C., Russell J.K., Moss S. 2009. Origin of olivine in kimberlite: phenocryst or impostor? *Lithos*, **112**(Suppl. 1):201-212. https://doi.org/10.1016/j.lithos.2009.04.030

Brod J.A., Gibson S.A., Thompson R.N., Junqueira-Brod T.C., Seer H.J., Moraes L.C., Boaventura G.R. 2000. The Kamafugite-Carbonatite association in the Alto Paranaíba Igneous Province (APIP) Southeastern Brazil. *Revista Brasileira de Geociências*, **30**(3):408-412. https://doi.org/10.25249/0375-7536.2000303408412

Bussweiler Y., Brey G.P., Pearson D.G., Stachel T., Stern R.A., Hardman M.F., Kjarsgaard B.A., Jackson S.E. 2017. The aluminum-in-olivine thermometer for mantle peridotites – Experimental versus empirical calibration and potential applications. *Lithos*, **272-273**:301-314. https://doi.org/10.1016/j.lithos.2016.12.015

Bussweiler Y., Foley S.F., Prelevic D., Jacob D.E. 2015. The olivine macrocryst problem: New insights from minor and trace element compositions of olivine from Lac de Gras kimberlites, Canada. *Lithos*, **220-223**:238-252. https://doi.org/10.1016/j.lithos.2015.02.016

Cabral Neto I., Nannini F., Silveira F.V., Cunha L.M. 2017. *Áreas kimberlíticas e diamantíferas do Estado de Minas Gerais: Informe de Recursos Minerais Complementar ao Mapa das Áreas Kimberlíticas e Diamantíferas do Estado de Minas Gerais e Regiões Adjacentes*. Brasília, Serviço Geológico do Brasil, 230 p.

Canil D. 1999. The Ni-in-garnet geothermometer: Calibration at natural abundances. *Contributions to Mineralogy and Petrology*, **136**(3):240-246. https://doi.org/10.1007/s004100050535

Canil D., Bellis A.J. 2007. Ferric iron in CaTiO3 perovskite as an oxygen barometer for kimberlite magmas II: Applications. *Journal of Petrology*, **48**(2):231-252. https://doi.org/10.1093/petrology/egl067

Canil D., Fedortchouk Y. 2001. Olivine-liquid partitioning of vanadium and other trace elements, with applications to modern and ancient picrites. *Canadian Mineralogist*, **39**(2):319-330. https://doi.org/10.2113/gscanmin.39.2.319

Carlson R.W., Esperança S., Svisero D.P. 1996. Chemical and Os isotopic study of Cretaceous potassic rocks from Southern Brazil. *Contributions to Mineralogy and Petrology*, **125**(4):393-405. https://doi.org/10.1007/s004100050230

Carmichael I.S.E. 1991. The redox states of basic and silicic magmas: a reflection of their source regions? *Contributions to Mineralogy and Petrology*, **106**:129-141. https://doi.org/10.1007/BF00306429

Carmichael I.S.E., Ghiorso M.S. 1986. Oxidation-reduction relations in basic magma: a case for homogeneous equilibria. *Earth and Planetary Science Letters*, **78**(2-3):200-210. https://doi.org/10.1016/0012-821X(86)90061-0

Carmichael I.S.E., Nicholls J. 1967. Iron-titanium oxides and oxygen fugacities in volcanic rocks. *Journal of Geophysical Research*, **72**(18):4665-4687. https://doi.org/10.1029/JZ072i018p04665

Cas R.A.F., Hayman P., Pittari A., Porritt L. 2008. Some major problems with existing models and terminology associated with kimberlite pipes from a volcanological perspective, and some suggestions. *Journal of Volcanology and Geothermal Research*, **174**(1-3):209-225. https://doi.org/10.1016/j.jvolgeores.2007.12.031

Chakhmouradian A.R., Mitchell R.H. 2000. Occurrence, alteration patterns and compositional variation of perovskite in kimberlites. *Canadian Mineralogist*, **38**(4):975-994. https://doi.org/10.2113/gscanmin.38.4.975

Clement C.R. 1982. *A Comparative Geological Study of Some Major Kimberlite Pipes in the Northern Cape and Orange Free State*. PhD Thesis, University of Cape Town, 432 p.

Comin-Chiaramonti P., Gomes C.B. 2005. *Mesozoic to Cenozoic Alkaline Magmatism in the Brazilian Platform*. São Paulo, Edusp/Fapesp, 750 p.

Costa G.V. 2008. *Química Mineral e Geotermobarometria de Xenólitos Mantélicos do Kimberlito Canastra-01*. MS Dissertation, Universidade de Brasília, Brasília, 137 p.

Costa V.S., Figueiredo B.R., Weska R.K. 1997. Estudos mineralógicos e químicos do kimberlito Batovi 6 (MT) em comparação com as intrusões Três Ranchos 4 (GO) e Limeira 1 (MG). *Geochimica Brasiliensis*, **11**(1):53-71. https://doi.org/10.21715/gb.v11i1.118

Dongre A., Tappe S. 2019. Kimberlite and carbonatite dykes within the Premier diatreme root (Cullinan Diamond Mine, South Africa): New insights to mineralogical-genetic classifications and magma CO2 degassing. *Lithos*, **338-339**:155-173. https://doi.org/10.1016/j.lithos.2019.04.020

Fedortchouk Y., Canil D. 2004. Intensive variables in kimberlite magmas, Lac de Gras, Canada and implications for diamond survival. *Journal of Petrology*, **45**(9):1725-1745. https://doi.org/10.1093/petrology/egh031

Fedortchouk Y., Canil D. 2009. Diamond oxidation at atmospheric pressure: development of surface features and the effect of oxygen fugacity. *European Journal of Mineralogy*, **21**(3):623-635. https://doi.org/10.1127/0935-1221/2009/0021-1929

Fedortchouk Y., Canil D., Carlson J.A. 2005. Dissolution forms in Lac de Gras diamonds and their relationship to the temperature and redox state of kimberlite magma. *Contributions to Mineralogy and Petrology*, **150**(1):54-69. https://doi.org/10.1007/s00410-005-0003-1

Felgate M.R. 2014. *The petrogenesis of Brazilian kimberlites and kamafugites intruded along the 125º lineament: Improved Geochemical and Geochronological Constraints on Magmatism in Rondonia and The Alto Paranaiba Igneous Province*. PhD Thesis, University of Melbourne, 275 p.

Foley S.F., Prelevic D., Rehfeldt T., Jacob D.E. 2013. Minor and trace elements in olivines as probes into early igneous and mantle melting processes. *Earth and Planetary Science Letters*, **363**:181-191. https://doi.org/10.1016/j.epsl.2012.11.025

Gibson S.A., Thompson R.N., Dickin A.P., Leonardos O.H. 1995a. High-Ti and low-Ti mafic potassic magmas: Key to plume - lithosphere interactions and continental flood-basalt genesis. *Earth and Planetary Science Letters*, **136**(3-4):149-165. https://doi.org/10.1016/0012-821X(95)00179-G

Gibson S.A., Thompson R.N., Leonardos O.H., Dickin A.P., Mitchell J.G. 1995b. The late cretaceous impact of the trindade mantle plume: Evidence from large-volume, mafic, potassic magmatism in SE Brazil. *Journal of Petrology*, **36**(1):189-229. https://doi.org/10.1093/petrology/36.1.189

Golubkova A.B., Nosova A.A., Larionova Y.O. 2013. Mg-ilmenite megacrysts from the Arkhangelsk kimberlites, Russia: genesis and interaction with kimberlite melt and postkimberlite fluid. *Geochemistry International*, **51**:353-381. https://doi.org/10.1134/S0016702913030038

Gonzaga G.M., Tompkins L.A. 1991. Geologia do diamante. *In*: Schobbenhaus C., Queiroz E.T. de, Coelho C.E.S. (eds.). *Principais depósitos minerais do Brasil - Gemas e rochas ornamentais*, p. 53-116. Brasília, DNPM/CPRM. v. 4.

Grütter H., Latti D., Menzies A. 2006. Cr-saturation arrays in concentrate garnet compositions from kimberlite and their use in mantle barometry. *Journal of Petrology*, **47**(4):801-820. https://doi.org/10.1093/petrology/egi096

Grütter H.S., Gurney J.J., Menzies A.H., Winter F. 2004. An updated classification scheme for mantle-derived garnet, for use by diamond explorers. *Lithos*, **77**(1):841-857. https://dx.doi.org/10.1016/j.lithos.2004.04.012

Guarino V., Wu F.Y., Lustrino M., Melluso L., Brotzu P., Gomes C.B., Ruberti E., Tassinari C.C.G., Svisero D.P. 2013. U-Pb ages, Sr-Nd- isotope geochemistry, and petrogenesis of kimberlites, kamafugites and phlogopite-picrites of the Alto Paranaíba Igneous Province, Brazil. *Chemical Geology*, **353**:65-82. https://doi.org/10.1016/j.chemgeo.2012.06.016

Gurney J.J., Zweistra P. 1995. The interpretation of the major element compositions of mantle minerals in diamond exploration. *Journal of Geochemical Exploration*, **53**(1-3):293-309. https://doi.org/10.1016/0375-6742(94)00021-3

Haggerty S.E. 1983. The mineral chemistry of new titanates from the Jagersfontein kimberlite, South Africa: implications for metasomatism in the upper mantle. *Geochimica et Cosmochimica Acta*, **47**(11):1833-1854. https://doi.org/10.1016/0016-7037(83)90201-6

Junqueira-Brod T.C., Brod J.A., Gaspar J.C., Jost H. 2004. Kamafugitic diatremes: facies characterisation and genesis – examples from the Goiás Alkaline Province, Brazil. *Lithos*, **76**(1-4):261-282. https://doi.org/10.1016/j.lithos.2004.03.037

Junqueira-Brod T.C., Roig H.L., Gaspar J.C., Brod J.A., Meneses P.R. 2002. A Província Alcalina de Goiás e a extensão de seu vulcanismo kamafugítico. *Revista Brasileira de Geociências*, **32**(4):559-566.

Kavanagh J.L., Sparks R.S.J. 2009. Temperature changes in ascending kimberlite magma. *Earth and Planetary Science Letters*, **286**:404-413. http://dx.doi.org/10.1016/j.epsl.2009.07.011

Le Maitre R.W. 2002. *Classification and nomenclature, in Igneous Rocks: a Classification and Glossary of Terms*. Cambridge, Cambridge University Press, 236 p.

Le Pioufle A., Canil D. 2012. Iron in monticellite as an oxygen barometer for kimberlite magmas. *Contributions to Mineralogy and Petrology*, **163**(6):1033-1046. http://dx.doi.org/10.1007/s00410-011-0714-4

Leonardos O.H., Carvalho J.B., Tallarico F.H.B., Gibson S.A., Thompson R.N., Meyer H.O.A., Dickin A.P. 1993. O xenólito de granada Iherzolito de Três Ranchos 4: uma rocha matriz do diamante na província magmática cretacea do Alto Paranaíba. *In*: I Simpósio de Geologia do Diamante, 1., 1993, Cuiabá. *Annals*..., p. 3-16.

Leonardos O.H., Meyer H.O.A. 1991. Outline of the geology of western Minas Gerais. *In*: International Kimberlite Conference, 5., 1991, Araxá. *Annals* ..., p. 8.

Locock A.J., Mitchell R.H. 2018. Perovskite classification: An Excel spreadsheet to determine and depict end-member proportions for the perovskite-and vapnikite-subgroups of the perovskite supergroup. *Computers & Geosciences*, **113**:106-114. https://doi.org/10.1016/j.cageo.2018.01.012

Malarkey J., Pearson D.G., Kjarsgaard B.A., Davidson J.P., Nowell G.M., Ottley C.J., Stammer J. 2010. From source to crust: tracing magmatic evolution in a kimberlite and a melilitite using microsample geochemistry. *Earth and Planetary Science Letters*, **299**(1-2):80-90. https://doi.org/10.1016/j.epsl.2010.08.020

Melluso L., Lustrino M., Ruberti E., Brotzu P., Gomes C.B., Morbidelli L., Morra V., Svisero D.P., Amelio F.D. 2008. Major- and trace-element composition of olivine, perovskite, clinopyroxene, cr–fe–ti oxides, phlogopite and host kamafugites and kimberlites, alto paranaíba, Brazil. *The Canadian Mineralogist*, **46**(1):19-40. https://doi.org/10.3749/canmin.46.1.19

Meyer H.O.A., Garwood B.L., Svisero D.P., Smith C.B. 1994. Alkaline ultrabasic intrusions in western Minas Gerais Brazil. *In*: International Kimberlite Conference, 5., 1994, Araxá. *Annals* ..., p. 140-155.

Meyer H.O.A., Svisero D.P. 1980. Kimberlites and diamonds in Brazil: Windows to the upper mantle. *Anais da Academia Brasileira de Ciências*, **52**:819-825.

Mitchell R.H. 1986. *Kimberlites: mineralogy, geochemestry, and petrology*. New York, Springer Science+Business Media, 442 p.

Mitchell R.H. 1995. *Kimberlites, Orangeites, and Related Rocks*. New York, Springer Science+Business Media, 410 p.

Mitchell R.H. 1997. *Kimberlite, Orangeites, Lamproites, Melilitites and Minettes: A Petrographic Atlas*. Winnipeg, Almaz Press Inc., 243 p.

Mitchell R.H. 2008. Petrology of hypabyssal kimberlites: Relevance to primary magma compositions. *Journal of Volcanology and Geothermal Research*, **174**(1-3):1-8. https://doi.org/10.1016/j.jvolgeores.2007.12.024

Mitchell R.H., Chakhmouradian A.R. 1998. Th-rich loparite from the Khibina alkaline complex, Kola Peninsula: isomorphism and paragenesis. *Mineralogical Magazine*, **62**(3):341-353.

Mori P.E., Reeves S., Correia C.T., Haukka M. 1999. Development of a fused glass disc XRF Facility and comparison with the pressed powder pellet technique at Instituto de Geociências, São Paulo University, Brazil. *Revista Brasileira de Geociências*, **29**(3):441-446. https://doi.org/10.25249/0375-7536.199929441446

Morimoto N. 1990. Nomenclatura de piroxênios. *Revista Brasileira de Geociências*, **20**(1-4):318-328.

Nimis P., Grütter H. 2010. Internally consistent geothermometers for garnet peridotites and pyroxenites. *Contributions to Mineralogy and Petrology*, **159**(3):411-427. https://doi.org/10.1007/s00410-009-0455-9

Nimis P., Taylor W.R. 2000. Single clinopyroxene thermobarometry for garnet peridotites. Part I. Calibration and testing of a Cr-in-Cpx barometer and an enstatite-in-Cpx thermometer. *Contributions to Mineralogy and Petrology*, **139**:541-554. https://doi.org/10.1007/s004100000156

Nowicki T.E., Moore R.O., Gurney J.J., Baumgartner M.C. 2007. Diamonds and Associated Heavy Minerals in Kimberlite: A Review of Key Concepts and Applications. *Developments in Sedimentology*, **58**:1235-1267. https://dx.doi.org/10.1016/S0070-4571(07)58046-5

Ogilvie-Harris R.C., Field M., Sparks R.S.J., Walter M.J. 2009. Perovskite from the Dutoitspan kimberlite, Kimberley, South Africa: implications for magmatic processes. *Mineralogical Magazine*, **73**(6):915-928. https://doi.org/10.1180/minmag.2009.073.6.915

Pollack H.N., Chapman D.S. 1977. On the regional variation of heat flow, geotherms, and lithospheric thickness. *Tectonophysics*, **38**(3-4):279-296. https://doi.org/10.1016/0040-1951(77)90215-3

Read G., Grutter H., Winter S., Luckman N., Gaunt F., Thomsen F. 2004. Stratigraphic relations, kimberlite emplacement and lithospheric thermal evolution, Quirico Basin, Minas Gerais State, Brazil. *Lithos*, **77**(1-4):803-818. https://doi.org/10.1016/j.lithos.2004.04.011

Riccomini C., Velázquez V.F., Gomes C.B. 2005. Tectonic controls of the Mesozoic and Cenozoic alkaline magmatism in central-southeastern Brazilian platform. *In*: Comin-Chiaramonti P., Gomes C.B. (eds.). *Mesozoic to Cenozoic Alkaline Magmatism in the Brazilian Platform*, p. 31-55. São Paulo, Edusp/Fapesp.

Robinson D.N. 1979. *Surface Textures and Other Features of Diamonds*. PhD Thesis, University of Cape Town, 161 p.

Sarkar C., Storey C.D., Hawkesworth C.J. 2013. Detailed Protracted Crystallization History of Perovskite in Orapa Kimberlite. *In*: International Kimberlite Conference, 10., 2013. *Extended abstracts*..., p. 211-224.

Sertek J.P., Andrade S., Ulbrich H.H. 2015. An Evaluation of the Effects of Primary and Cross-Contamination during the Preparation of Rock Powders for Chemical Determinations. *Geostandards and Geoanalytical Research*, **39**(3):381-397. https://doi.org/10.1111/j.1751-908X.2014.00324.x

Sparks R.S.J. 2013. Kimberlite Volcanism. *Annual Review of Earth and Planetary Sciences*, **41**:497-528. https://doi.org/10.1146/annurev-earth-042711-105252

Sparks R.S.J., Baker L., Brown R.J., Field M., Schumacher J., Stripp G., Walters A. 2006. Dynamical constraints on kimberlite volcanism. *Journal of Volcanology and Geothermal Research*, **155**(1-2):18-48. https://doi.org/10.1016/j.jvolgeores.2006.02.010

Stachel T., Luth R.W. 2015. Diamond formation - Where, when and how? *Lithos*, **220-223**:200-220. https://doi.org/10.1016/j.lithos.2015.01.028

Stagno V., Ojwang D.O., McCammon C.A., Frost D.J. 2013. The oxidation state of the mantle and the extraction of carbon from Earth's interior. *Nature*, **493**:84-90. https://doi.org/10.1038/nature11679

Svisero D.P., Haralyi N.L.E., Girardi V.A.V. 1980. Geologia dos kimberlitos Limeira 1, Limeira 2 e Indaiá, Douradoquara, MG. *In*: Congresso Brasileiro de Geologia, 31., 1980, Balneário de Camboriú, Santa Catarina. *Annals* ..., p. 1789-1801.

Svisero D.P., Meyer H.O.A., Haralyi N.L.E., Hasui Y. 1984. A Note on the Geology of Some Brazilian Kimberlites. *The Journal of Geology*, **92**(3):331-338.

Talukdar D, Chalapathi Rao NV. 2015. Diamond Prospectivity of Mesoproterozoic kimberlites from the Wajrakarur field, southern India: perovskite oxybarometry and bulk-rock transition element geochemistry constraints. *Journal of Indian Geophysical Union*, **19**(2):175-181.

Trickett S.K. 2007. *Mapping lithofacies within the D/K1 kimberlite Pipe at Letlhakane, Botswana: An assessment of petrgraphic, geochemical and mineralogical indicators*. PhD Thesis, University of London, London.

Ubide T., Arranz E., Lago M., Galé C., Larrea P. 2012. The influence of crystal settling on the compositional zoning of a thin lamprophyre sill: A multi-method approach. *Lithos*, **132-133**:37-49. https://doi.org/10.1016/j.lithos.2011.11.012

Zhang Z. 2016. *Diamond resorption morphology as a fluid proxy in diamond-bearing environments: constraints from empirical and experimental studies*. PhD Thesis, Dalhousie University, Nova Scotia.